Eur. Phys. J. B **38**, 49–58 (2004)
DOI: 10.1140/epjb/e2004-00098-8

THE EUROPEAN PHYSICAL JOURNAL B

The anisotropic quantum antiferromagnet on the Sierpiński gasket: Ground state and thermodynamics

A. Voigt[1,a], W. Wenzel[2], J. Richter[3], and P. Tomczak[4]

[1] Center for Simulational Physics, Department of Physics and Astronomy, University of Georgia, Athens GA 30602, USA and Max-Planck-Institut Magdeburg, Sandtorstr.1, 39106 Magdeburg, Germany
[2] Forschungszentrum Karlsruhe, Institut für Nanotechnologie, Postfach 3640, 76021 Karlsruhe, Germany
[3] Otto-von-Guericke-Universität Magdeburg, Institut für Theoretische Physik, PF 4120, 39106 Magdeburg, Germany
[4] Uniwersytet im. Adama Mickiewicza, Wydział Fizyki, ul.Umultowska 85, 61-614 Poznań, Poland

Received 8 December 2003 / Received in final form 18 February 2004
Published online 20 April 2004 –

Abstract. We investigate an antiferromagnetic $s = 1/2$ quantum spin system with anisotropic spin exchange on a fractal lattice, the Sierpiński gasket. We introduce a novel approximative numerical method, the configuration selective diagonalization (CSD) and apply this method to a the Sierpiński gasket with $N = 42$. Using this and other methods we calculate ground state energies, spin gap, spin–spin correlations and specific heat data and conclude that the $s = 1/2$ quantum antiferromagnet on the Sierpiński gasket shows a disordered magnetic ground state with a very short correlation length of $\xi \approx 1$ and an, albeit very small, spin gap. This conclusion holds for Heisenberg as well a for XY exchange.

PACS. 75.10.-b General theory and models of magnetic ordering – 05.45.Df Fractals – 75.40.Mg Numerical simulation studies

1 Introduction

Low-dimensional quantum antiferromagnets (AFM) have been intensively investigated since the development of quantum mechanics in the early twenties [1]. A renewed interest was motivated by the discovery of high-temperature superconductivity [2] and the peculiar interplay of the magnetic and electronic properties of these systems, where antiferromagnetism and superconductivity appear in close vicinity (see e.g. [3] and Ref. therein). Since then various experimental findings for materials for electronically one- or twodimensional magnetic systems, such as CuGeO CaVO, SrCuBO, have called for more detailed theoretical investigations of the ground state and the low temperature properties of one- and two-dimensional quantum AFM (see e.g. [4] and ref. therein). Despite many theoretical efforts, many properties of low-dimensional quantum AFM, in particular the interplay of quantum fluctuations and magnetic order near quantum critical points, need further explanation.

The radical difference in the behavior of one- and two-dimensional AFM has been subject of current debate, in particular with regard to its interaction with changes in the lattice structure (in the cuprates), the presence of spin-peierls transitions or the influence of disorder. One of the most significant dimension-dependent properties is the type of magnetic order: the ground state of the one-dimensional $s = 1/2$ Heisenberg chain remains disordered [1], but for the two–dimensional Heisenberg quantum AFM on square, triangular or honeycomb lattices one observes a Néel-like magnetic long range order in the ground state. The dimensional crossover between $d = 1$ and $d = 2$ has been studied via investigations of ladder structures [5] or by varying exchange parameters on two–dimensional lattices (e.g. on the square lattice or on the triangular lattice) [6–12].

In addition to the dimensionality the spin anisotropy can also influence the magnetic order in quantum AFM. For example, it is known that in the one–dimensional linear chain an infinitesimal small Ising-like exchange anisotropy induces a Néel-like magnetic order in the ground state. In zig-zag ladders the effects of XY anisotropy may lead to spiral ordering [13]. For two–dimensional lattices at finite temperatures (where the Mermin-Wagner theorem forbids any Néel–like long-range order for pure Heisenberg exchange) an XY exchange anisotropy can induce a vortex type ordering at the Kosterlitz-Thouless transition [14].

We have previously studied the influence of dimensionality on the magnetic order by considering a quantum AFM on a particular lattice geometry, the Sierpiński gasket, with a topological dimension between one and two. We considered a Heisenberg interaction between the nearest-neighbor spins on this lattice and investigated its properties with exact diagonalization and variational wave functions [15,16]. We supplemented this analysis with

[a] e-mail: voigt@mpi-magdeburg.mpg.de

thermodynamical properties using the quantum decimation technique (QDT) [17] and a decoupled-cell Monte-Carlo approach (DCM) [18]. Recently we extended this research to higher spins [19] as well as to anisotropic spin interactions [20]. From all calculated data we have presented arguments in favor of a disordered ground state of the Sierpiński gasket quantum AFM.

All mentioned numerical approaches have some limitations and disadvantages. The exact diagonalization is subject to the well known constraint on the system size. Its application to quantum spin models is always challenging but in the case of a fractal lattice even more complicated due to loss of translational symmetries. Therefore only small systems with $N = 15$ could be investigated so far (In [20] we include a system with $N = 28$, which has a similar topology like $N = 15$ but is in fact not a true Sierpiński gasket). The variational wave function calculations suffer from the uncertainties in the reference wavefunction due to lattice frustration and the thermodynamical properties calculated with QDT and DCM might not probe the true ground state. Therefore all previous conclusions have been drawn with particular care and indeed, especially the investigation of larger systems is very desirable for further support and verification.

In this paper we will apply a new technique, the configuration selective diagonalization (CSD), in a particular efficient implementation to investigate larger finite lattices. This approach is based on ideas developed in quantum chemistry [21,22] and evolves around an extrapolative calculation of the ground state and low excitations. Using this approach we are able to access larger systems in a numerically controlled approximation. We will present results for the $N = 42$ Sierpiński gasket (the next larger Sierpiński gasket after $N = 15$) for both the Heisenberg and the XY model. This is to our knowledge the largest quantum spin system treated so far with a direct diagonalization technique. The treatment of this cluster permits the analysis of spin-spin correlations for larger lattice separations and allows us to further strengthen the predictions of a disordered ground state for the Heisenberg model. It also enables us to draw similar conclusions for the XY model on the Sierpiński gasket.

In Section 2 we will introduce the model and its basic properties. In Section 3 we present all numerical methods used in our investigation. We will emphasize on the CSD in very detail, as this is the first application of this approach to quantum spin systems. In Section 4 the results of the calculations will be presented and conclusions about the magnetic order behavior will be made. We summarize the paper in Section 5.

2 The model

We consider the quantum $s = 1/2$ AFM with anisotropic spin exchange:

$$\hat{H} = J \sum_{\langle i,j \rangle} \left(\mathbf{S}_i^x \mathbf{S}_j^x + \mathbf{S}_i^y \mathbf{S}_j^y + \Delta \mathbf{S}_i^z \mathbf{S}_j^z \right). \qquad (1)$$

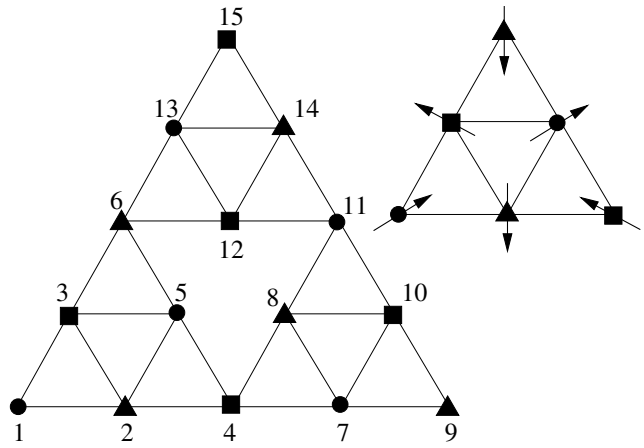

Fig. 1. Left: The classical ground state configuration of the $N = 15$ Sierpiński gasket with 3 sublattices: A (circles), B (squares) and C (triangle). Right: The spin direction in the classical ground state with an angle of 120° between spins belonging to different sublattices.

The antiferromagnetic spin exchange $J > 0$ is taken between nearest neighbors on the Sierpiński gasket (an example of this lattice with $N = 15$ is given in Fig. 1). The anisotropy Δ will be studied for the Heisenberg model at $\Delta = 1$ and for the XY model at $\Delta = 0$. The most important geometrical property of the Sierpiński gasket is its fractal Hausdorff dimension of $d_f = \frac{\ln(3)}{\ln(2)} \approx 1.58$. The number of spins on this lattice is given by $N = \frac{1}{2}(3^n + 3)$ with $n = 1, 2, 3, \ldots$. In the paper we will focus on $N = 6$, 15 and 42 (i.e. $n = 2, 3, 4$).

The classical ground state is a planar spin state with 3 sublattices for $\Delta \leq 1$. The spins in such a sublattice are ferromagnetically aligned, between spins belonging to different sublattices we observe an angle of 120°. This ground state is depicted by the arrows in the right part of Figure 1. The classical ground state of the Sierpiński gasket is analogous to the ground state of the two–dimensional triangular lattice and has no non-trivial degeneracy.

We would like to mention here that there is an ongoing debate of the relation between the properties of the classical ground state and the magnetic order of the quantum ground state. For the *kagomé* lattice it was argued in [23] that the infinite degeneracy of the classical ground state is closely connected to the high number of low-lying singlets in the quantum case (and therefore maybe to a liquid-like quantum ground state.) Ongoing research did show that there are systems like the planar pyrochlore lattice with a classical non-trivial degeneracy of the ground state, yet with valence bond type long range order in the quantum regime [24]. The multi-spin exchange model is another counter example with **no** non-trivial classical degeneracy but with a large number of low lying singlets [25]. As it has been discussed already in [19] the Sierpiński gasket is yet another example as it has **no** non-trivial classical degeneracy, even though in the quantum case it also shows a large number of low-lying singlets and a disordered liquid-like ground state.

3 The methods

In this paper we will use a variety of methods to investigate the Sierpiński gasket. For finite quantum AFM of small size the exact diagonalization (ED) with a Lanczos approach is the tool of choice to investigate the ground state and the low energy spectrum. Because of the exponentially growing Hilbert space the approach is usually limited to systems with up to $N = 36$, only for highly symmetric lattices like the square lattice one can reach $N = 40$ [26,27]. As already stated the CSD will be used for the calculation of the ground state and first excited state of the $N = 42$ Sierpiński gasket. For thermodynamic properties we will deploy a complete diagonalization (CD) for smaller finite systems and a quantum decimation technique (QDT).

Whereas the complete diagonalization is routinely used (for more information see e.g. [28]), the QDT is not known to a wide audience even though it has been successfully implemented to investigate low-temperature thermodynamics of different low–dimensional AFM [29,30]. Therefore we will shortly describe the two basic steps of this approach on the example of the Sierpiński gasket. In the first step, one splits the Hamiltonian H of an infinite system into Hamiltonians H_i of finite 6-spin subsystems (see right part of Fig. 1) ($H = \sum_i H_i$). Recalling that the renormalization group (RG) procedure should preserve the partition function and symmetry of the system and, additionally, the decimation procedure should preserve the correlation function, one traces out some spin degrees of freedom in each finite subsystem. In the second step one puts these finite subsystems together and obtains a renormalized Hamiltonian H':

$$\exp\left(\sum_i H_i\right) \approx \prod_i \exp(H_i) \approx \prod_i \exp(H_i') \approx \exp\left(\sum_i H_i'\right).$$

Note that while splitting the Hamiltonian into finite subsystems and subsequently replacing the true local Hamiltonian by the renormalized H_i' one neglects the non-commutativity of the spin operators.

This two-step RG transformation enables one to calculate the free energy per spin as follows:

$$-f/k_BT = \sum_{i=0}^{\infty} \left(\frac{1}{3}\right)^i g(K^{(i)}), \qquad (2)$$

with $K^{(i)}$ representing the i-times transformed coupling constant $K \equiv J/k_BT$ (k_B – Boltzmann constant and T – temperature). The g in the above equation represents the contribution to the free energy (per spin) from degrees of freedom which have been decimated out in one RG transformation. For additional details of this method see for e.g. [17,30].

As already stated the CSD will be used for the first time for quantum spin systems and we therefore describe it now in very detail.

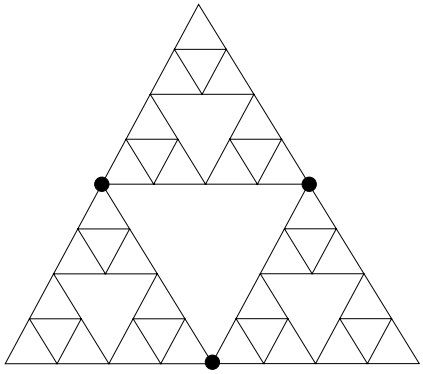

Fig. 2. 42 Site approximant of the Sierpiński gasket. If the sites indicated by black circles are treated as a central fragment, the remainder of the system decomposes into three uncoupled thirteen-site satellite fragments.

3.1 Configuration selective diagonalization

As noted above exact diagonalization methods are limited to small systems because of an the exponential increase of the Hilbert space with the system size. In certain circumstances, however, the size of treatable systems may be increased significantly if only approximate energies and expectation values are required. Here we describe the adaptation of the CSD for the approximative calculation of low-energy properties of quantum spin systems in the context of the $N = 42$ Sierpiński gasket. This approach has been developed using the methodology recently applied in the multi-configuration interaction methods [22,31,32] in quantum chemistry. In the following, we will describe this method and its implementation for the system at hand, but note that it is applicable to other systems as well. The division of the whole system into fragments which are exactly solvable within an exact Lanczos diagonalization is a necessary precondition for the application of the CSD, as discussed in detail below.

The model in Figure 2 contains 42 sites, resulting in a Hilbert space of dimension 5.3×10^{11} in the $S_z^{tot} = 0$ subspace, which can be reduced by a factor of approximately four by discrete Abelian symmetries, such as spin- and real-space reflection. The use of the three-fold rotation incurs too much computational overhead to be of real value. Even so, it remains too large for exact diagonalization schemes for low-lying eigenstates. The special structure of the cluster permits the use of approximate configuration-selective diagonalization methods. If we subdivide the cluster into a central fragment containing the three sites indicated with black dots, its remainder consists of three identical "satellite" fragments of 13 sites each. If there were no bonds between the central fragment and the satellites, the eigenstates of the overall system would be outer products of the eigenstates of the four fragments. In the presence of interactions, only four bonds couple the central fragment with each of the satellites, which may be assumed to perturb the spectrum of the satellites only weakly. Because the satellite fragments are only weakly coupled to the central system, it is plausible

to expand the eigenstate of the overall system in a basis of outer products of eigenstates of the satellite fragments. In the absence of any coupling to the central fragment, this approximation would be exact, in their presence one can hope that only a few configuration in this expansion will carry the overwhelming weight of the wavefunction. This observation suggests the application of the CSD (which has a long history in similar scenarios in quantum chemistry [21,33]) to quantum spin systems.

The basic idea of this approach is simple: Suppose an approximate wavefunction of the ground state is already known and this wavefunction has nonzero coefficients only for a small fraction of the configurations of the Hilbert space. We then estimate the weight of each remaining unselected configuration in second order perturbation theory. We keep only such configurations where the absolute value of the estimated coefficient surpasses a predefined threshold ϵ and sum the perturbative energy contributions of the neglected configurations. Next we determine the eigenstate within the new selected Hilbert space with a direct diagonalization technique. The resulting state will be a better approximation of the desired eigenstate in the full Hilbert space. These two steps are alternated with decreasing selection threshold ϵ and the energy (including the perturbative correction of the discarded configurations) and other expectation values are extrapolated to the limit $\epsilon \to 0$. For many systems this limit can be safely extrapolated with selected Hilbert spaces that contain only a small fraction of the possible configurations. The process is initiated with some simple trial wavefunction containing only the appropriate ground-state configurations of the segments.

The algorithm thus consists of two distinct phases: in the *expansion step* new configurations are selected perturbatively and in the *diagonalization step* the lowest (or a few of the lowest) eigenvalues of the selected Hilbert space are determined. In the *diagonalization step* we iteratively improve a trial vector for the ground state of the selected Hilbert space using a preconditioned Davidson method [34,35]. The time-consuming step of this iterative method is the computation of expectation values $\langle \Psi_i | H | \Psi_j \rangle$ of the many body Hamiltonian H between trial states

$$|\Psi_i\rangle = \sum_k \alpha_{ik} |\phi_k\rangle , \tag{3}$$

where $|\phi_k\rangle$ designate the configurations of the selected Hilbert space. The evaluation of such matrix elements is difficult, because at any given stage, the selected Hilbert space contains an essentially random subset of the possible configurations.

The Hamilton operator H of the system can be written as

$$H = H_c + \sum_s H_s + \sum_s H_{sc} \tag{4}$$

where s enumerates the satellite fragments and c designates the central fragment. H_s and H_c sum terms of H acting on a single fragment, while H_{sc} couples the satellite s to the central fragment.

To evaluate the expectation values we pre-diagonalize the 13-site satellite fragments in their respective S_z^{tot} spin-segments and compute the boundary-operators $S_{sb}^{\pm}$ and S_{sb}^{z} for the four boundary sites b of each fragment s in this basis. Similarly we compute the matrix representation of the corresponding operators for the central fragment. Each configuration $|\phi_k\rangle$ in the Hilbert space is labeled by a quadruplet of quantum numbers (n_c, n_1, n_2, n_3), where n_i is the index of an eigenstate of the corresponding fragment. The first two terms in the Hamiltonian (4) are diagonal in this representation and easily evaluated.

Nondiagonal terms, in contrast, are difficult to evaluate because of the sparsity of the selected configurations in the overall Hilbert space. In order to avoid costly lookup operations we have developed a so-called residue based scheme for the evaluation of the matrix elements that we will describe in detail in the following. Each coupling term H_{sc} is a sum of products of pairs of boundary operators described above. To efficiently evaluate the expectation values of this part of the Hamiltonian we use a residue based matrix element evaluation technique that was originally developed for selecting configurations in interaction methods [22,31].

For a particular configuration of the selected Hilbert space one individual term in H_{cs} changes the quantum numbers on the central fragment and on one of the satellite fragments (in the following we choose without loss of generality fragment 1). The quantum numbers on the other two fragments n_2, n_3 are the same on the right- and left-hand side of the configuration for nonzero matrix elements. All all nonzero contributions arising from this particular term in the Hamiltonian connect two configurations which have the same index n_2, n_3. Since we wish to enumerate all nonzero matrix elements, we can use this set as a label for the associated matrix elements. In the following we will call this set of quantum numbers of both configurations the transition residue (R) mediating the matrix element. For each transition residue (n_2, n_3) we can enumerate the configurations that lead to nonzero matrix elements by a doubly nested *residue tree*.

All nonzero matrix elements mediated by a particular transition residue R are uniquely enumerated by pairs of indices of the first level and pairs of indices of the second level of the residue tree R. There are no matrix elements spanning different residue trees. As an example the matrix element evaluation for $H_{sc} = S_c^+ S_1^-$ can thus be written as:

$$\langle \Psi_1 | H_{cs} | \Psi_2 \rangle = \sum_{R=(n_2,n_3)} \sum_{c_1,c_2 \text{in Tree } R} S^+_{c_1 c_2} \left(\sum_{s_1 \text{in list } (R,c_1)} \sum_{s_2 \text{in list } (R,c_2)} A^{(1)*}_{(R,c_1,s_1)} S^-_{s_1 s_2} A^{(2)}_{(R,c_2,s_2)} \right) . \tag{5}$$

In order to carry out the sums in the above equation, we construct a *residue tree* for each $R = (n_2, n_3)$, which is

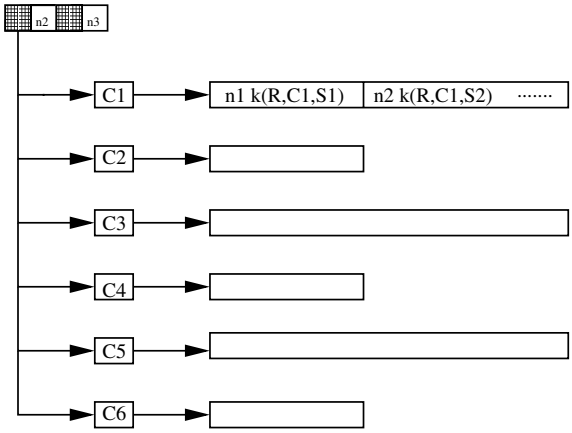

Fig. 3. A single entry R in the residue tree (top left) is designated by the quantum numbers of the fragment not changed by the operator in question (see text, (n_2, n_3) in the example). The first level labels the quantum number of the central fragment that is necessary to completely specify the state. Attached to each such entry c_i is the list of indices of the configurations that have quantum numbers $(c_i, \ldots, n_2, n_3)$. Each element of such a list contains the quantum number n_1 of the configuration and its associated index of the coefficient of the associated configurations $k(R, c_i, s)$.

illustrated schematically in Figure 3. The first level of the tree enumerates the allowed quantum numbers of the central fragment $(n_c = c_1, c_2, c_3, \ldots)$. The second level of the tree enumerates for each central fragment quantum number the selected configurations (c_i, s_j, n_2, n_3) and contains the value of the coefficient of the associated configuration: $A(R = (n_2, n_3), c_i, s_j,)$. The sum in equation (5) is then computed by picking all allowed pairs of branches c_j, c_j of the tree. For each pair of branches, each pair of entries generates a nonzero matrix element. This double sum can thus be performed without further lookup operations and evaluates nevertheless only matrix elements that connect *selected configurations*. Note that the innermost loops run over all selected indices on the satellites, i.e. encode $\mathrm{O}(N_s^2)$ operations for a fully selected Hilbert space, where $N_s \approx 1000$ is the dimension of the Hilbert space on a satellite fragment. In order to build the tree just once for many applications of the Hamiltonian, it is more efficient to store the indices $k(R, c_2, s_2)$ rather than the coefficients in the tree.

Using this procedure all matrix elements can be evaluated for arbitrarily complicated subspaces without lookup operations. We have implemented the residue tree by nested Adelson-Vleski-Landes (AVL) balanced binary trees which permit O(log(N)) read/write operations per access. The numerical effort associated with building the residue tree is then proportional to the number of configurations. The number of matrix elements encoded by the tree, however is proportional to the expectation value of the square of the lengths of the inner subtrees, i.e. the inner sum in equation (5). This sum scales with the number of configurations on a satellite fragment ($O(N_s^2)$ for the fully selected case. As a result this matrix evaluation scheme is very efficient, in tests the expectation values were computed 200 times faster than with a traditional hash-table based implementation. This increase in the numerical efficiency permits the treatment of much larger Hilbert spaces.

Since the different residue trees are independent of one another, we can implement a relatively simple, scalable parallelization of the matrix element evaluation on a limited number of nodes, by distributing the residue trees across the nodes. In our implementation using 8 nodes of an SGI Power Challenge incurred a total loss of about 12% of CPU time compared with a run on a single node. This loss of efficiency results from the fact that the number of matrix elements encoded by a given residue tree depends on the number of configurations containing its residue quantum numbers.

In the *expansion step* for a given reference state $|\Psi\rangle$ we diagonalize

$$\begin{pmatrix} \langle\Psi|H|\Psi\rangle & \langle\Psi|H|\phi_i\rangle \\ \langle\phi_i|H|\Psi\rangle & \langle\phi_i|H|\phi_i\rangle \end{pmatrix} \tag{6}$$

for each trial configuration $|\phi_i\rangle$ and use its coefficient for the selection criterion. If the new configurations $|\phi_i\rangle$ were mutually non-interacting this would generate the exact eigenstate of the system. The time consuming step in the diagonalization of equation (6) is the computation of the off-diagonal coupling matrix element $\langle\phi_i|H|\Psi\rangle$ between the reference state and the trial configuration, which can be accomplished using a similar residue based scheme as for the evaluation of the matrix elements. Initially we choose a small subset of configurations with the lowest energies which is diagonalized exactly. The lowest eigenstate of this Hilbert space is used as the reference state for the first iteration, for subsequent iterations the converged state of the previous iteration is used.

For the present system, however, it is not feasible to even consider all possible trial configurations ($N = \mathrm{O}\,(10^{11})$) in the expansion loop. In each expansion step we therefore proceed as follows: first we order the configurations of the last state by the absolute weight of their coefficients. We then generate the interacting configurations for the most important configurations until the total weight of the configurations considered in the reference state exceeds about 90% of its norm. *Interacting configurations* of a given configuration are all those that have a nonzero matrix element with the Hilbert space of the selected configurations. These are typically only a small fraction (about 1−3%) of the selected configurations. For these configurations we apply the selection criteria and gather the selected subset containing n_1 new configurations. We then generate the interacting configurations of the next important segment of the reference state until to total weight of the configurations of the reference state exceeds 96% of its norm and generate n_2 new configurations from this set. We continue this process with geometrically decreasing fraction of the norm until the number of newly generated configurations n_k is less than 5% of the total number of newly generated configurations $n_1 + n_2 + \cdots + n_{k-1}$. Since configurations with very little

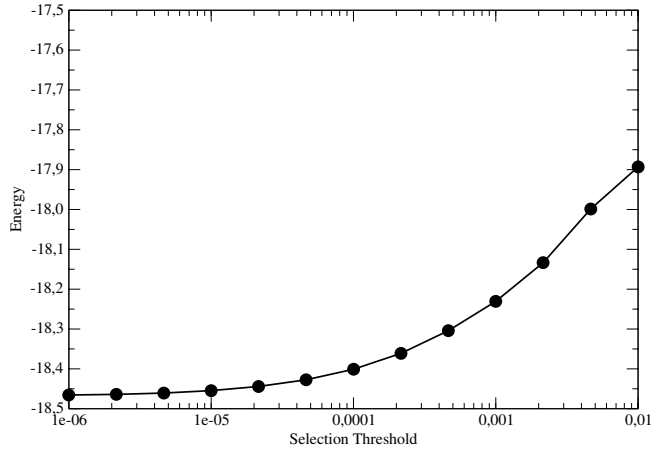

Fig. 4. Convergence of the energy as a function of the selection threshold.

weight in the original wavefunction are unlikely to generate interacting configurations that will be selected we avoid to even build the full interacting space of the reference wavefunction.

Figure 4 illustrates the convergence of the ground state energy with respect to the selection threshold for the system at hand. It demonstrates that for selection thresholds less then 1×10^{-5} the energy is extrapolated with an accuracy of one percent or better.

Expectation values, such as correlation functions can be easily computed by adapting the residue driven scheme. One constructs residue trees corresponding to the appropriate operators and evaluates the expectation values similar to the energy.

4 Results

4.1 Spin-spin correlations

We turn now to the investigation of the ground state magnetic order on the *quantum* $s = 1/2$ antiferromagnetic Sierpiński gasket. The careful investigation of the spin–spin correlations $\langle S_i S_j \rangle$ will provide a deeper insight into the ordering behavior.

We begin with the ground state energy (being just the sum over all nearest-neighbor spin–spin correlations on the Sierpiński gasket). In the following table we provide the calculated value of the ground state energy for all finite lattices up to $N = 42$. We provide the site and the bond average energies (This might help other groups to compare to our data.)

In a quantum spin system with Néel-like semi-classical ordering the spin–spin correlation between the spins in one classical sublattice remains constant for large distances after a slight decay due to the quantum fluctuations. Therefore we first investigate the spin–spin correlations between the spins of one classical sublattice as defined in Section 2 (for example all sites with circles ● in Fig. 1).

The geometrical distance, which is normally the measure on one- or two-dimensional lattices, is not easily transferable to fractal objects, such as the Sierpiński gasket. For the Sierpiński gasket we therefore use the Manhattan distance r_M which counts the minimal number of steps required to connect one site to the other. Because of lack of translational symmetry in the Sierpiński gasket we find different spin–spin correlations between spins having the same Manhattan distance. In what follows we use a simple averaging procedure over all spin–spin correlations at a given Manhattan distance.

Table 1. Number of spins N, site energy e_s and bond energy e_b for the Sierpiński gaskets up to $N = 42$. (For $N = 42$ the error of the CSD calculation is given in brackets.)

N	Heisenberg		XY	
	e_s	e_b	e_s	e_b
6	-0.375	-0.25	-0.25	$-0.16666\bar{6}$
15	-0.416125	-0.231181	-0.282024	-0.156680
42	$-0.439(5)$	$-0.227(9)$	$-0.298(8)$	$-0.154(9)$

In our earlier investigations we predicted a disordered ground state using the exact diagonalization data for $N = 15$ among others. Below we will compare this data with the new data for $N = 42$ to confirm our prediction. In Figure 5 the spin–spin correlation $\langle S_i S_j \rangle_{i,j\in\bullet}$ for the Sierpiński gasket (SG) with $N = 42$ and corresponding data for a two-dimensional square lattice (SL) with $N = 40$ [26,27] (where magnetic long-range order is well known to exist) is shown. For the SL data we have chosen the shell distance r_S (where shell-like circles numbered 1,2,3, ... are drawn around a given site which then connect all neighbors at the given distance).

The Sierpiński gasket shows a dramatic drop in the spin–spin correlations and for large distances it even changes its sign. This is in marked contrast to the two-dimensional square lattice where after a slight decrease due to the quantum fluctuations an almost constant behavior over distance is observed. This points to a complete loss of the classical Néel-like magnetic order in the quantum Heisenberg AFM on the Sierpiński gasket. Almost the same behavior can be seen for the XY model with $\Delta = 0$. Here we have to distinguish between the different components of the spin–spin correlation due to the spin anisotropy: $\langle S_i^x S_j^x \rangle = \langle S_i^y S_j^y \rangle \neq \langle S_i^z S_j^z \rangle$. But as one can see the different components of the spin–spin correlations show similar behavior and the complete loss of any classical Néel-like magnetic order.

Even though the classical magnetic order seems to be absent, some other type of long-range order in the pair correlations might prevail in the Sierpiński gasket. In order to check this conjecture we calculate the absolute spin–spin correlation $|\langle S_i S_j \rangle|_{i,j\in N}$ between *all* spins (and not just between spins in a classical sublattices) over r_M (again using an averaging procedure as described above) and show a semilogarithmic plot of the data.

From Figure 6 we deduce that only very short ranged correlations exist at all in the Sierpiński gasket and this behavior is independent of the spin anisotropy. For the XY model (right) we observe again a similar behavior

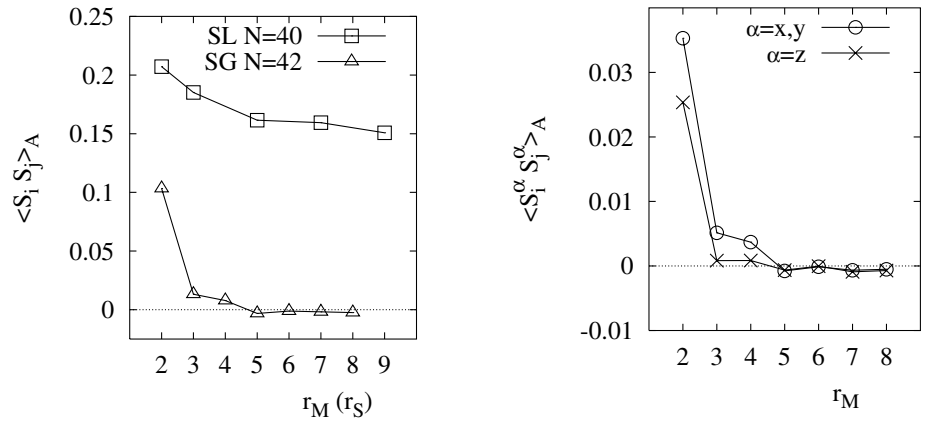

Fig. 5. The spin–spin correlation between spins on a classical sublattice $\langle S_i S_j \rangle_{i,j\in\bullet}$ vs. distance. Left: $\Delta = 1$ (Heisenberg model) – data for the Sierpiński gasket with $N = 42$ (SG) vs. Manhattan distance r_M and corresponding data for a two-dimensional square lattices with $N = 40$ (SL) vs. the shell distance r_S; Right: $\Delta = 0$ (XY model) – data for the Sierpiński gasket with $N = 42$ for the x- and z-components of $\langle S_i S_j \rangle$.

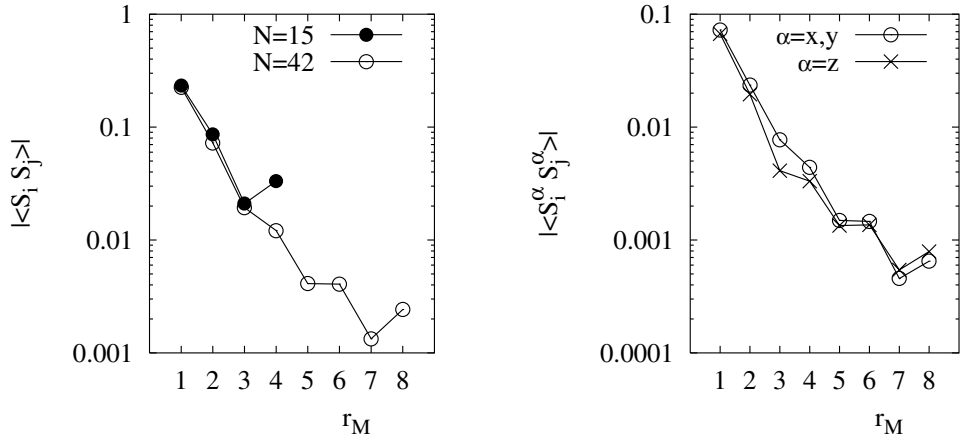

Fig. 6. The average of all absolute spin–spin correlations $\overline{|\langle S_i S_j \rangle|}_{i,j\in N}$ vs. Manhattan distance r_M of the Sierpiński gasket. Left: $\Delta = 1$ (Heisenberg model) – $\overline{|\langle S_i S_j \rangle|}$ for $N = 15$ and $N = 42$; Right: $\Delta = 0$ (XY model) – $\overline{|\langle S_i^x S_j^x \rangle|}$ and $\overline{|\langle S_i^z S_j^z \rangle|}$ for $N = 42$.

for the different components of the spin–spin correlation. From the semilogarithmic plot we derive a correlation length $\xi \approx 1$, applying $|\langle S_i S_j \rangle| \sim e^{-(r_M/\xi)}$. The very small (in absolute values) upturn of the spin–spin correlations for the largest separation is presumably a boundary effect of the corner spins of the Sierpiński gasket. These corner spins have a different coordination number (only 2 bonds instead of 4) and they are mainly contributing to the value of this particular spin–spin correlation.

As we observe only short range order in the Sierpiński gasket, we turn to the investigation of the local order which might exist in this lattice. We show in Figure 7 the spin–spin correlations on the Sierpiński gasket bonds only and chose $\langle S_i^z S_j^z \rangle$ (Heisenberg case) and $\langle S_i^x S_j^x \rangle$ (XY case). The other components behave quite similar.

We observe in the Heisenberg case (left) as well as in the XY case (right) a tendency to a plaquette formation at the corner spins. An example of such a plaquette is seen between the spins 39-40-42-41. Here the spin–spin correlations are very pronounced between the neighbor spins on the assumed plaquette (and reach about 80% of the true isolated plaquette value as we have checked) and they are apparently much smaller to the remaining lattice (where for an isolated plaquette we would observe 0). And even though there is an antiferromagnetic bond between the spins 40 and 41, the resulting spin–spin correlation between this two spins is ferromagnetic which points to a beginning dimer formation between them. The other dimer correlation $\langle S_{39} S_{42} \rangle$ (value not shown in Fig. 7) is 0.234 (Heisenberg case) and 0.230 (XY case) and therefore very close to a true dimer correlation of 1/4. One could argue that another plaquette may form inside the lattice (one example might be spins 30-31-34-33). We have found a similar behavior already for the $N = 15$ Sierpiński gasket. The building of plaquettes in a lattice with strong frustration seems quite interesting given the fact that in the strong frustrated region of the $J_1 - J_2$ square lattice model one might find a similar behavior (although this behavior is still under controversial discussion) [36–38].

4.2 Spin gap

In this section we investigate the spin gap Γ, defined as

$$\Gamma = E(S^z_{min} + 1) - E(S^z_{min}). \tag{7}$$

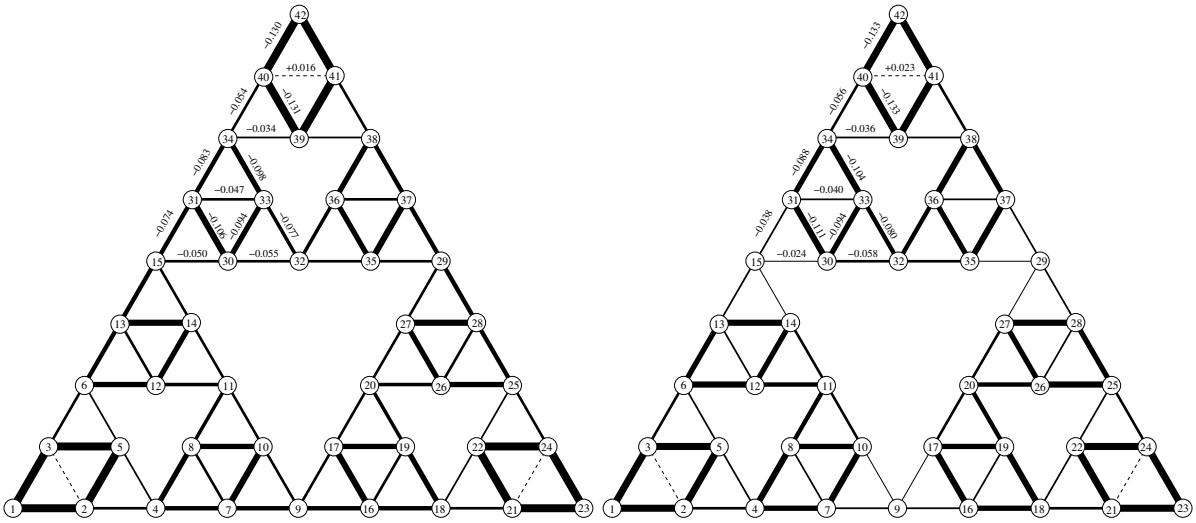

Fig. 7. The nearest neighbor spin–spin correlation on the Sierpiński gasket with $N = 42$. Left: $\Delta = 1$ (Heisenberg model) – $\langle S_i^z S_j^z \rangle$, Right: $\Delta = 0$ (XY model) – $\langle S_i^x S_j^x \rangle$ (The dotted lines stand for a ferromagnetic correlation.)

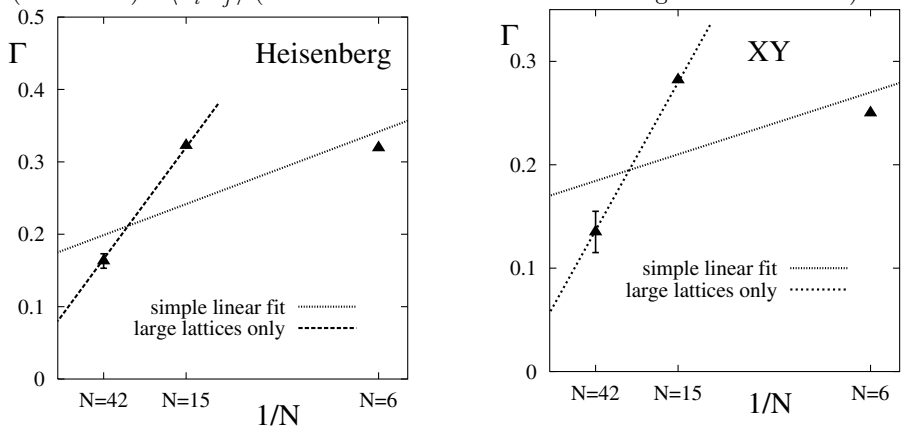

Fig. 8. The spin gap vs. inverse system size for the Sierpiński gasket with $N = 6$,15 and 42. Left: $\Delta = 1$ (Heisenberg model); Right: $\Delta = 0$ (XY model).

The absence of Néel–like magnetic long-range order is as a rule accompanied by a finite spin gap and can therefore be used as another criterion for a disordered ground state [39]. In Figure 8 we present Γ for the Heisenberg and XY case.

The data for $N = 6$ and 15 has been presented before but with the CSD we are able to calculate the spin gap for $N = 42$ as well. The data has to be analyzed with particular care, because we expect finite size effects still to be present. If we just make a simple linear fit through the data we roughly get a value $\Gamma \approx 0.2$. One might also argue that $N = 6$ is too small to be taken into account for this consideration and therefore we did another fit with only $N = 15$ and 42. Still we see that the spin gap Γ remains finite, but is reduced to $\Gamma \approx 0.1$. A similar conclusion holds for the XY model, although the spin gap appears to be smaller (this behavior has been found in other investigations too [40]). Though our finite-size extrapolation must be taken with particular care we see further arguments in favor of a finite spin gap and a ground state without magnetic long–range order.

We mention that the AFM on the Sierpiński gasket belongs to the class of frustrated spin systems (like the *kagomé* or the checkerboard lattices) having exactly known localized magnon eigenstates leading to a macroscopic magnetization jump to saturation [41,42]. These localized magnons can live e.g. on 'hexagons' (large triangles) inside satellite fragment (e.g. the sites 4,5,6,12,11,8 in Fig. 7). For $N = 42$ the magnetization jumps at the saturation field $h_{sat} = 3J$ from $m = 17/21$ to saturation $m = 1$. Even for N $\to \infty$ the height of the jump remains finite since the number of localized magnons occupying the lattice grows with N.

4.3 Low temperature thermodynamics

It is known that the low-temperature specific heat is closely related to the low-lying excitations of a system [4,43–45]. As we have argued already in Section 4.2 the low-lying excitations in turn might show a spin gap behavior and therefore point to a disordered ground state. We and others have seen in previous investigations a close

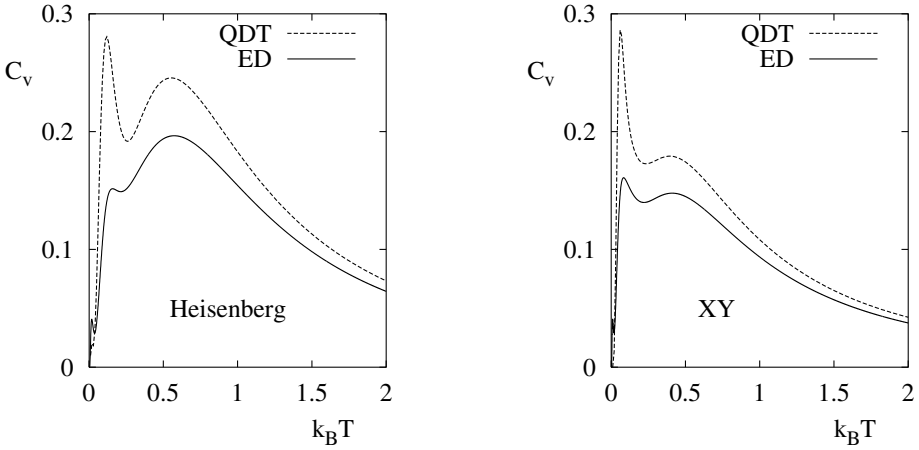

Fig. 9. The low temperature specific heat: full diagonalization data for the $N = 15$ system and quantum decimation data. Left: $\Delta = 1$ (Heisenberg model); Right: $\Delta = 0$ (XY model).

connection between an additional low-temperature peak in the specific heat and a finite spin gap [18,44,46,47]. Following this argumentation we will analyze the specific heat c_v of the system especially in its low-temperature region. We show in Figure 9 c_v for the Heisenberg and XY Sierpiński gasket calculated with CD and QDT. We note that the c_v results for the Heisenberg case are identical to those of reference [17] and shown for comparison purposes.

We observe in both cases additional low-temperature peaks which relate to two different energy scales relevant in the system. The first energy scale is connected to the typical broad peak, whereas the second one is connected to the low-temperature peak and its value is connected to the finite spin gap Γ_∞. This behavior of the specific heat is typical for all antiferromagnetic systems on "corner sharing triangles" lattices (*kagomé* [44], *Sierpiński* [17], *squagome* [30]). In fact, in all those systems the basic unit leading to this behavior is a Δ-chain [46,47] which *shares* spins with other Δ-chains. (*kagomé* – 12 spin chain, *Sierpiński* – 6 spin chain, *squagome* – 8 spin chain). The RG transformation used here takes into account the excitation spectrum of 6 spin chain (Fig. 1, right) and by using equation (2) one gets a larger low-temperature peak in comparison to exact diagonalization data.

In both cases an additional low-temperature peak in the specific heat constitutes an additional argument for a finite spin gap and therefore for a disordered ground state. The small additional peak in the exact diagonalization data at even lower temperatures has been attributed to a finite size effect [19].

5 Summary

We have carried out a numerical investigation of a $s = 1/2$ quantum antiferromagnet on the Sierpiński gasket with two types of spin exchange, Heisenberg and XY. We have used the exact diagonalization, a newly implemented configuration selective diagonalization approach and a quantum decimation technique to calculate the spin–spin correlations in the ground state, the spin gap and the low-temperature specific heat.

The current investigation complements and verifies previous work done for the Sierpiński gasket [15–20]. Main progress in the investigation of this fractal many-body system results from the successful introduction of the configuration selective diagonalization (CSD). This new method permits the calculation of the ground state wavefunction (and therefore all correlation functions) and excited states as well for larger finite quantum spin system. Using CSD we calculated the spin–spin correlations and the spin gap for $N = 42$. We note that the method can be applied to other frustrated low–dimensional quantum spin systems with just moderate changes.

The reported data suggest that the ground state of the Sierpiński gasket remains disordered for Heisenberg and XY spin exchange. It seems that the interplay of quantum fluctuations and low dimension prevents any kind of magnetic long range order in this system. From the available data we derive a magnetic correlation length $\xi \approx 1$. The nearest-neighbor spin–spin correlations show a tendency to plaquette formation. It will be interesting to find out whether or not this behavior is related to similar findings in the strongly frustrated region of the $J_1 - J_2$ Heisenberg antiferromagnet.

A.V. is grateful to the Institute of Molecular Physics of the Polish Academy of Sciences in Poznań (Poland) for kind hospitality during his stay. This work was supported by the DFG under Grant-Nr. Ri 615/5-1, KBN Grant-Nr. PO3B 046 14 and by NSF grant ACI-0081789.

References

1. H. Bethe, Z. f. Phys. **71**, 205 (1931)
2. J.G. Bednorz, K.A. Müller, Z. f. Phys. B **64**, 188 (1986)
3. E. Manousakis, Rev. Mod. Phys. **63**, 1 (1991)
4. C. Lhuillier, G. Misguich, *Frustrated quantum magnets*, Lecture Notes in Physics, Vol. 595 (Springer, Heidelberg, 2002), pp. 161–190

5. E. Dagotto, T.M. Rice, Science **271**, 618 (1996)
6. I. Affleck, M.P. Gelfand, R.R. Singh, J. Phys. A **27**, 7313 (1994)
7. D. Ihle, C. Schindelin, A. Weisse, H. Fehske, Phys. Rev. B **60**, 9240 (1999)
8. O.A. Starykh, R.R.P. Singh, G.C. Levine, Phys. Rev. Lett. **88**, 167203 (2002)
9. P. Sindzingre, J.-B. Fouet, C. Lhuillier, Phys. Rev. B **66**, 174424 (2002)
10. A.A. Nersesyan, A.M. Tsvelik, Phys. Rev. B **67**, 024422 (2003)
11. W. Brenig, M. Grzeschik, `cond-mat/0304382`, 2003
12. P. Sindzingre, Phys. Rev. B **69**, 094418 (2004)
13. A.A. Nersesyan, A.O. Gogolin, F.H.L. Essler, Phys. Rev. Lett. **81**, 190 (1998)
14. J.M. Kosterlitz, D.J. Thouless, J. Phys. **6**, 1181 (1973)
15. P. Tomczak, A.R. Ferchmin, J. Richter, in *Coherent Approaches to Fluctuations* (World Scientific, 1996), p. 284
16. P. Tomczak, A.R. Ferchmin, J. Richter, Phys. Rev. B **54**, 395 (1996)
17. P. Tomczak, Phys. Rev. B **53**, R500 (1996)
18. A. Voigt, J. Richter, P. Tomczak, J. Magn. Magn. Mater. **183**, 68 (1998)
19. A. Voigt, J. Richter, P. Tomczak, Physica A **299**, 107 (2001)
20. A. Voigt, J. Richter, in *Advances in Quantum Many-Body Theory*, Vol. 6 (World Scientific, 2002), p. 111
21. R.J. Buenker, S.D. Peyerimhoff, Theor. Chim. Acta. **35**, 33 (1974)
22. P. Stampfuss, W. Wenzel, H. Keiter, J. Comput. Chem. **20**, 1559 (1999)
23. P. Lecheminant, B. Bernu, C. Lhuillier, L. Pierre, P. Sindzingre, Phys. Rev. B **56**, 2521 (1997)
24. J.-B. Fouet, M. Mambrini, P. Sindzingre, C. Lhuillier, Phys. Rev. B **67**, 54411 (2003)
25. P. Sindzingre, W. LiMing, G. Misguich, C. Lhuillier, Phys. Rev. B **62**, 6372 (2000)
26. A. Honecker, J. Schulenburg, J. Richter, J. Phys.: Condens. Matter **16**, 749 (2004)
27. J. Richter, J. Schulenburg, A Honecker, to be published
28. W.H. Press, S.A. Teukolsky, W.T. Vetterling, B.P. Flannery, *Numerical Recipes in FORTRAN* (Cambridge University Press, Cambridge, 1992)
29. P. Tomczak, J. Richter, Phys. Rev. B **54**, 9004 (1996)
30. P. Tomczak, J. Richter, J. Phys. A **36**, 5399 (2003)
31. F. Stephan, W. Wenzel, J. Chem. Phys. **108**, 1015 (1998)
32. P. Stampfuss, W. Wenzel, submitted to J. Chem. Phys. (2003)
33. Z. Gershgorn, I. Shavitt, Int. J. Quant. Chem. **2**, 751 (1968)
34. E.R. Davidson, Adv. Quantum Chem. **6**, 235 (1972)
35. J. Olsen, P. Jorgensen, J. Simons, Chem. Phys. Lett. **169**, 463 (1990)
36. R.R.P Singh, Z. Weihong, C.J. Hamer, J. Oitmaa, Phys. Rev. B **60**, 7278 (1999)
37. L. Capriotti, S. Sorella, Phys. Rev. Lett. **84**, 3137 (2000)
38. L. Capriotti, F. Becca, A. Parola, S. Sorella, Phys. Rev. Lett. **87**, 97201 (2001)
39. A. Auerbach, *Interacting Electrons and Quantum Magnetism* (Springer Verlag, Berlin, 1994)
40. P. Tomczak, J. Richter, J. Phys. A **34**, L461 (2001)
41. J. Schulenburg, A. Honecker, J. Schnack, J. Richter, H.-J. Schmidt, Phys. Rev. Lett. **88**, 167207 (2002)
42. J. Richter, J. Schulenburg, A. Honecker, J. Schnack, H.-J. Schmidt, J. Phys.: Condens. Matter **16**, 779 (2004)
43. G. Misguich, C. Lhuillier, B. Bernu, C. Waldtmann. Phys. Rev. B **60**, 1064 (1999)
44. P. Sindzingre, G. Misguich, C. Lhuillier, B. Bernu, L. Pierre, Ch. Waldtmann, H.-U. Everts, Phys. Rev. Lett. **84**, 2953–6 (2000)
45. C. Lhuillier, P. Sindzingre, J.-B. Fouet, Can. J. Phys. **79**, 1525 (2001)
46. K. Kubo, Phys. Rev. B **48**, 10552 (1993)
47. T. Nakamura, K. Kubo, Phys. Rev. B **53**, 6393 (1996)